# Template-Synthesized $LiCoO_2$, $LiMn_2O_4$, and $LiNi_{0.8}Co_{0.2}O_2$ Nanotubes as the Cathode Materials of Lithium Ion Batteries

**Xiaoxia Li, Fangyi Cheng, Bing Guo, and Jun Chen***

*Institute of New Energy Material Chemistry, Nankai University, Tianjin 300071, People's Republic of China*

*Received: April 12, 2005; In Final Form: May 30, 2005*

The first point of this work is to synthesize $LiCoO_2$, $LiNi_{0.8}Co_{0.2}O_2$, and $LiMn_2O_4$ nanotubes with the template of porous anodic aluminum oxide by thermal decomposition of sol−gel precursors. The as-synthesized materials were open-ended nanotubes with uniform shape and size based on the analysis of scanning electron microscopy, transmission electron microscopy, and X-ray diffraction. An "in situ reaction from nanoparticle to nanotube" mechanism was discussed for the formation process of the nanotubes. The second point of this paper is to investigate the electrochemical properties of the as-synthesized nanotubes for the cathode materials of lithium ion batteries. It was found that the nanotube electrodes exhibited better reversibility and higher discharge capacities than that of their nanocrystalline counterparts. The reason for the improved electrochemical performance of the nanotube electrodes was also interpreted.

## Introduction

Rechargeable lithium ion batteries are becoming more and more important at both fundamental and applied levels because of their high energy density and design flexibility.[1,2] The capacity of these batteries is usually cathode (positive electrode)-limited, so it follows that increasing the capacity of the cathode is essential to raise the performance of such batteries. By far, the most common cathode active materials that are being researched and commercially used in lithium ion batteries are the lithiated transition metal oxides such as $LiCoO_2$, $LiNiO_2$, $LiMn_2O_4$, and the doped counterparts.[1−4]

The two-dimensional (2D) $LiCoO_2$ and $LiNiO_2$ adapt the $\alpha$-$NaFeO_2$ type structure, which can be regarded as a distorted rock salt superstructure.[5] The Li/$LiCoO_2$ cells undergo a transport process of lithium ions between anode and cathode (namely, rocking chair process) and exhibit very high voltages and specific energies.[6−8] Practically all of the lithium in $LiCoO_2$ can be removed electrochemically. However, reversible cycling can be carried out only in a limited range of composition. The reason is due to the high oxidizing power of the almost delithiated $Li_xCoO_2$ ($x < 0.3$), which causes corrosion and solvent decomposition problems.[9] As a comparison, the isostructural $LiNiO_2$ is attracting intense attention not only because of its economic advantage over $LiCoO_2$ but also due to its much lower redox potential, allowing it to be less prone to electrolyte oxidation.[10,11] Unfortunately, stoichiometric $LiNiO_2$ is difficult to obtain. Interestingly, the substitution of nickel in $LiNiO_2$ with cobalt has led to an almost strictly 2D structure with superior electrochemical performance, making the doped one a promising material as the positive electrode of lithium ion batteries.[12,13]

It is also reported that spinel $LiMn_2O_4$ with a three-dimensional crystal structure is at present a very prospective candidate for the cathode material of lithium ion batteries due to its low cost, acceptable environmental impact, and excellent voltage profile characteristics.[14,15] However, the cycling performance of $LiMn_2O_4$ is rather poor, which is attributed to an asymmetric lattice expansion/contraction of the $Li_{1-x}Mn_2O_4$ electrode during the discharge/charge reactions.[16] In comparison with layered oxides such as $LiCoO_2$ and $LiNiO_2$, the cycling capability and discharge capacity of $LiMn_2O_4$ need to be improved.

The rate-determining step in the electrodes of lithium ion batteries is supposed to be a solid state diffusion. The smaller the particle size is, the shorter the diffusion length is, and as a result, faster kinetics are expected.[17] It is demonstrated by different groups[18,19] that the capacities of $LiMn_2O_4$ electrodes were enhanced by decreasing the average grain size of the oxide. Furthermore, electrodes made with nanotubes should show possible advantages such as faster diffusion kinetics over nanoparticle electrodes. As Nishizawa et al. reported,[20] improvement of charge−discharge performance was achieved with the electrode of $LiMn_2O_4$/polypyrrole composite nanotubules. Besides, it was also displayed that template-synthesized $V_2O_5$ nanotube arrays possessed a high $Li^+$ intercalation capacity of 300 mAh/g, which was about twice that of $V_2O_5$ film.[21] Therefore, the discharge capacities, cycling life, and safety performance of rechargeable lithium ion batteries are dramatically affected by the particle size and surface morphology of the active materials making up the cathodes.

Recently, Zhou et al.[22−24] prepared ordered nanowires of lithiated transition metal oxides by the template method. However, to the best of our knowledge, no attempts have been made to fabricate the nanotubes of $LiCoO_2$ and doped $LiNiO_2$ or further test their electrochemical activity. Because the template method with porous membranes of anodic aluminum oxides (AAO) has been successfully used to prepare various nanotubes[25−27] and because the nanotubes electrodes may exhibit better electrochemical performances, here, we report on the synthesis of $LiCoO_2$, $LiNi_{0.8}Co_{0.2}O_2$, and $LiMn_2O_4$ nanotubes and their further studies in electrochemical lithium insertion/deinsertion. The results show that the electrodes made with these nanotubes exhibit high capacity, excellent high rate discharge performance, and supreme cycling reversibility, indicating that

* To whom correspondence should be addressed. Fax: +86-22-2350-9118. E-mail: chenabc@nankai.edu.cn.

10.1021/jp051900a CCC: $30.25 
Published on Web 06/30/2005

nanotubes of lithiated transition metal oxides are promising cathode active materials for advanced rechargeable lithium ion batteries.

## Experimental Section

**Preparation of Bulk Samples.** All chemicals were of analytical grade and used as purchased without further purification. A stoichiometric amount of nitrate salts (Li:Co = 1:1) was dissolved in deionized water and mixed well with ethylene glycol and then evaporated at 80 °C for 8 h to form transparent sol. The sol was prefired slowly to develop the gel, milled, and then calcined at different temperatures to form bulk $LiCoO_2$. A stoichiometric amount of nitrate salts (Li:Mn = 1:2, Li:Ni:Co = 1:0.8:0.2, and Li:Ni = 1:1) was also used as the precursors, and a similar process was adopted to prepare the corresponding sols and bulk product, respectively.

**Preparation of Nanotubes.** The nanotubes were template-synthesized by a thermal decomposition of the sol−gel precursors within the pores of AAO membrane (Whatman, Φ 47 mm with 200 nm pore and 60 $\mu$m thickness). The templates were dipped into the sol for 10 min and taken out for heating at 500 °C for 8 h in air atmosphere. The entire "dip−anneal−dip" process was repeated three times for each sample, resulting in the formation of nanotubes within the template pores. The resulting template composites were dissolved in 6 M NaOH solution to remove the alumina and to obtain self-sustained nanotubes, which were collected and rinsed with deionized water and absolute ethanol several times to get the final products.

**Characterization of Nanotubes.** The chemical compositions of transition metal and oxygen in the as-prepared specimens were analyzed by an inductively coupled plasma (ICP) emission spectroscopy (model P-5200 from Hitachi). The analysis of lithium content in the samples was carried out by an atomic absorption spectrometer (AA, Perkin-Elmer Inc.) with monochromatic radiation of a lithium lamp operating at $\lambda = 670$ nm. The phase purity of the products was characterized by powder X-ray diffraction (XRD, Rigaku D/max 2500 X-ray generator, Cu Kα radiation). The morphologies and microstructures of the as-synthesized nanotubes were investigated by scanning electron microscopy (SEM, Philips XL-30 and JEOL JSM-6700F Field Emission), transmission electron microscopy (TEM), and high-resolution TEM (HRTEM) with fast Fourier transformation (FFT) (Philips Tecnai T20ST, 200 kV). Specimens for TEM analysis were prepared by dropping the dilute alcohol dispersion of samples on the surface of a copper grid and allowing them to air dry before analysis. Specific surface areas were measured by Brunauer−Emmett−Teller (BET) nitrogen adsorption−desorption (Shimadzu, Micromeritics ASAP 2010 Instrument).

**Electrochemical Measurements.** Electrochemical measurements were carried out using two-electrode cells with lithium metal as the counter electrode. The working electrodes were fabricated by compressing the mixture of 85 wt % active materials ($LiCoO_2$, $LiNi_{0.8}Co_{0.2}O_2$, or $LiMn_2O_4$ nanotubes), 10 wt % acetylene black, and 5 wt % ploytetrafluoroethylene onto a copper film. The cell assembly was operated in a glovebox filled with pure argon (99.999%) in the presence of an oxygen scavenger and a sodium-drying agent. The electrolyte solution was 1 M $LiPF_6$ dissolved in a mixture of ethylene carbonate (EC), propylene carbonate (PC), and diethyl carbonate (DEC) with the volume ratio of EC:PC:DEC = 3:1:1. Electrochemical performance was investigated using a Solartron SI 1260 Potentionstat Analyzer with 1287 Interface and a modified Arbin charge−discharge unit at controlled temperatures. Cyclic voltammograms (CVs) were carried out at the scan rate of 1 mV/s and at 20 °C. All of the voltages are reported in this paper vs $Li/Li^+$. The electrochemical capacity of the electrode was measured by a galvanostatic discharge−charge method at a current density of 10, 20, or 40 mA/g and the temperature of 20 °C. Charge−discharge cycles were tested with a current density of 10 mA/g in the potential range between 3 and 4.3 V.

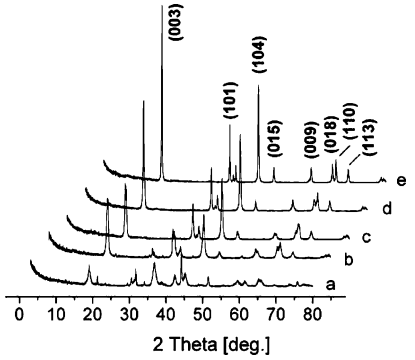


**Figure 1.** XRD patterns of bulk $LiCoO_2$ prepared in air at different temperatures (a) 300, (b) 400, (c) 500, (d) 600, and (e) 700 °C.

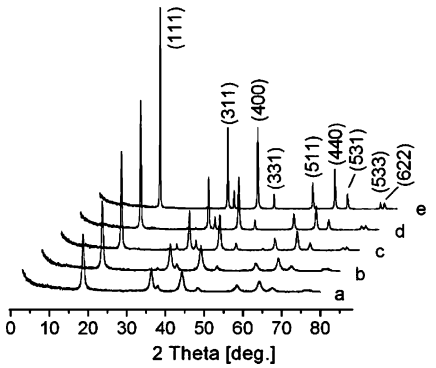


**Figure 2.** XRD patterns of bulk $LiMn_2O_4$ prepared in air at (a) 300, (b) 400, (c) 500, (d) 600, and (e) 700 °C.

## Results and Discussions

The synthesis of bulk $LiCoO_2$ and $LiMn_2O_4$ at different temperatures was first studied in order to get the light for preparing their corresponding nanotubes. Figure 1 shows the XRD data for bulk $LiCoO_2$ annealed from 300 to 700 °C. Figure 1a is the XRD pattern of the sample treated at 300 °C, showing the coexistence of $LiCoO_2$, $Li_2CO_3$, and $Co_3O_4$. The intermediates originated from the pyrolysis of the precursor. It was found that under the annealing temperature of 400 °C, $LiCoO_2$ formed as the dominant phase with little $Li_2CO_3$ and $Co_3O_4$ remaining, as shown in Figure 1b. This conformed to the fact that the reaction between $Li_2CO_3$ and $Co_3O_4$ can result in the formation of $LiCoO_2$.[28,29] XRD patterns of Figure 1c−e match well with the standard values of $LiCoO_2$ (ICDD-JCPDS card no. 44-145). The diffraction peaks of Figure 1d,e became shaper, displaying the fact of improved crystallization at elevated temperatures. Figure 2 shows that the XRD patterns of bulk $LiMn_2O_4$ annealed from 300 to 700 °C. It can be seen that all of the XRD patterns in Figure 2 are in good agreement with the standard values of spinel $LiMn_2O_4$ (ICDD-JCPDS card no. 35-782) with a cubic phase, indicating the relatively easy synthesis of single-phase $LiMn_2O_4$.[30,31] Meanwhile, the increase of the annealing temperature can enhance the crystallinity of the product. It should be noted that the actual processes involved in the synthesis of $LiCoO_2$ and $LiMn_2O_4$ were quite complex, and the in situ

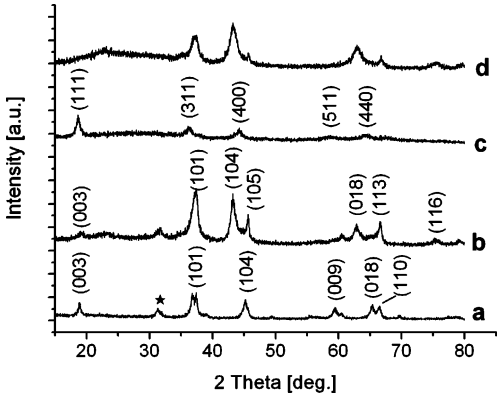


**Figure 3.** XRD patterns of nanotubes: (a) $LiCoO_2$ (peak with ★ is due to impurity), (b) $LiNi_{0.8}Co_{0.2}O_2$, (c) $LiMn_2O_4$, and (d) NiO (assumed to $LiNiO_2$).

reactions could be expressed simply as follows:

$$LiNO_3 + Co(NO_3)_2 + 2C_2H_6O_2 + 3/2O_2 \rightarrow LiCoO_2 + 4CO_2 + 6H_2O + 3/2N_2 \quad (1)$$

$$LiNO_3 + 2Mn(NO_3)_2 + 3C_2H_6O_2 + 2O_2 \rightarrow LiMn_2O_4 + 6CO_2 + 9H_2O + 5/2N_2 \quad (2)$$

On the basis of the above XRD analysis, it is reasonable to believe that similar reaction processes can occur in the synthesis of the $LiCoO_2$ and $LiMn_2O_4$ nanotubes as well as $LiNi_{0.8}Co_{0.2}O_2$ nanotubes with an AAO template. However, AAO membranes became difficult to remove after they were annealed over 600 °C due to the formation of $\gamma$-$Al_2O_3$, as confirmed in our experiments. Thus, the template synthesis of $LiCoO_2$, $LiNi_{0.8}Co_{0.2}O_2$, and $LiMn_2O_4$ and assumed $LiNiO_2$ nanotubes was performed at 500 °C. Figure 3 shows the XRD patterns of the corresponding as-prepared nanotubes. The XRD spectra of Figure 3a can be indexed to the hexagonal structure [space group: $R\bar{3}m$ (166)] with cell parameters $a = 2.817$ Å and $c = 14.037$ Å, in agreement with the standard values of $LiCoO_2$ (ICDD-JCPDS card no. 44-145). The as-prepared $LiNi_{0.8}Co_{0.2}O_2$ nanotubes (Figure 3b) are in the rhombohedral symmetry with lattice parameters $a = 2.955$ Å and $c = 14.425$ Å, which are a little larger than literature values.[32] The diffraction peaks in Figure 3c can be indexed to a spinel phase [space group: $Fd\bar{3}m$ (227)] with a lattice constant of $a = 8.212$ Å, which is compatible with the standard value of $LiMn_2O_4$ (ICDD-JCPDS card no. 35-782). It was reported that the nonstoichiometric $Li_{0.86}NiO_2$ phase could not be formed from $Li_2CO_3$ and NiO through the process performed for bulk $LiCoO_2$ until at a high temperature of 700 °C.[33] This was verified in our experiment that the product was NiO rather than $LiNiO_2$ at 500 °C (shown in Figure 3d). It is consistent with the fact that stoichiometric $LiNiO_2$ is difficult to synthesize. Therefore, we next address the characterization and electrochemical measurements of $LiCoO_2$, $LiNi_{0.8}Co_{0.2}O_2$, and $LiMn_2O_4$ nanotubes.

The chemical compositions of the as-prepared nanotubes were analyzed by AA and ICP, and it was found that the determination remained close to $LiCoO_2$, $LiNi_{0.8}Co_{0.2}O_2$, and $LiMn_2O_4$, which accords with the result of XRD measurement and further proves the purity of the as-synthesized nanotubes. To investigate the morphology information of the products, SEM images at different magnification were taken.

Figure 4 shows the representative SEM images of the as-obtained nanotubes. Figure 4a is a typical overall view of the $LiCoO_2$ tubes at a relatively low magnification. It indicates that a significant proportion (>95%) of the sample is present in straight tubular structure. A higher magnification image (Figure 4b) shows that the nanotubes are open-ended with a smooth surface. The typical length of these nanotubes is shorter than the thickness of the template (60 $\mu$m), which may owe to the ultrasonic treatment before SEM measurement. SEM images of Figure 4c,d display that the $LiNi_{0.8}Co_{0.2}O_2$ nanotubes have thick walls. As seen in Figure 4e,f, $LiMn_2O_4$ nanotubes pile up in disordered arrays with irregular tube tips, demonstrating the frangibility of the nanotubes. These frangible tubes are present in relatively shorter lengths; as a result, higher surface areas will be obtained. This was confirmed by BET measurement (see below). It's also noticed that $LiNi_{0.8}Co_{0.2}O_2$ and $LiMn_2O_4$ nanotubes exhibit coarse surfaces. We infer that this is attributed partly to the trace remaining alumina, which did not dissolve in NaOH solution, and, more decisively, the aggregation of smaller nanoparticles constituting the tube structure.

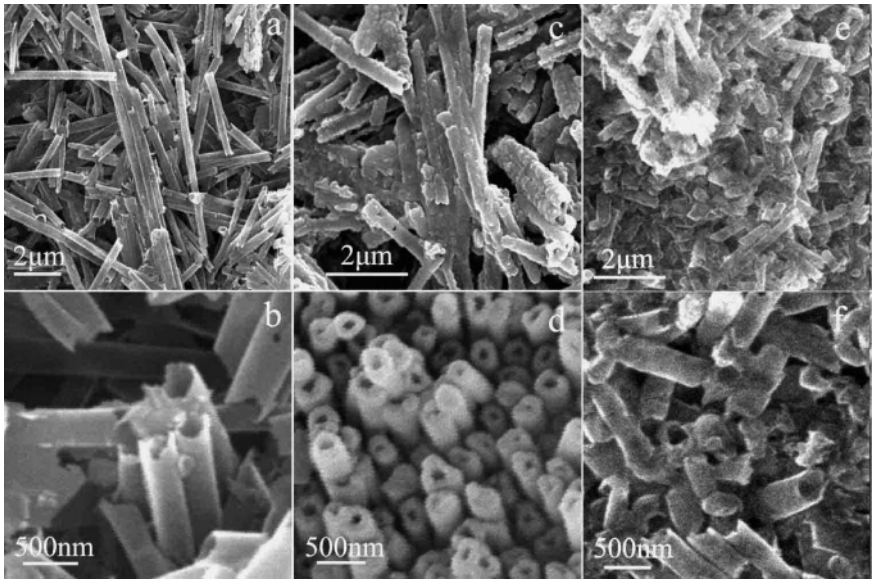


**Figure 4.** SEM images of (a) an overall view of $LiCoO_2$ nanotubes, (b) $LiCoO_2$ tubes with open tips, (c) an overall view of $LiNi_{0.8}Co_{0.2}O_2$ nanotubes, (d) face-on view of $LiNi_{0.8}Co_{0.2}O_2$ nanotube arrays with open-end tips, (e) $LiMn_2O_4$ nanotubes stacking up in disarray, and (f) $LiMn_2O_4$ tubes with open-ended tips.

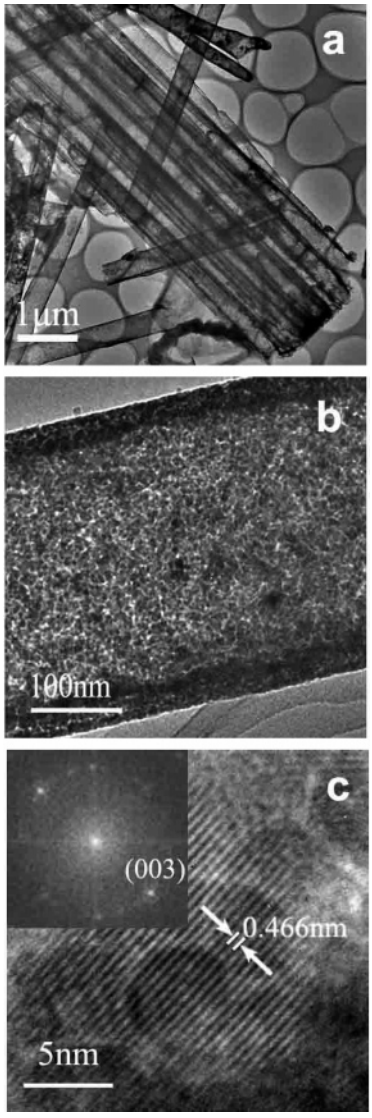


**Figure 5.** Representative TEM (a,b) and HRTEM (c) images of the as-prepared $LiCoO_2$ nanotube. The inset of panel c is the corresponding FFT analysis.

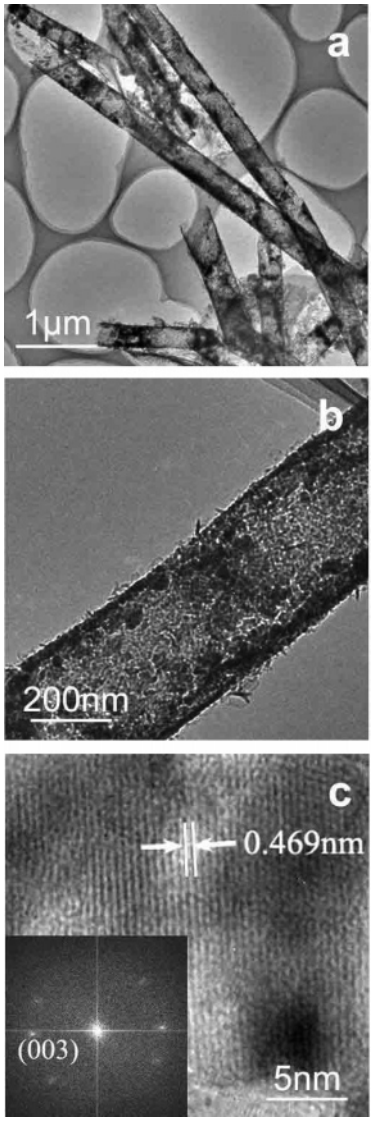


**Figure 6.** Representative TEM (a,b) and HRTEM (c) images of the as-prepared $LiNi_{0.8}Co_{0.2}O_2$ nanotubes. The inset of panel c is the corresponding FFT analysis.

To further understand the morphology and nanostructure details of the as-prepared lithiated transition metal oxides tubes, TEM and HRTEM were performed. The TEM image in Figure 5a is a bundle of $LiCoO_2$ nanotubes scattering on the copper mesh. The magnified image (Figure 5b) confirms the tubular structure with the bright central part contrasting their dark edges. As shown in Figure 5b, the nanotubules extend the complete thickness of the template membrane used. A layer separation of 0.466 nm, which corresponds to (003) planes in bulk $LiCoO_2$, was observed in the HRTEM image (Figure 5c).

Figure 6 shows the TEM and HRTEM images of $LiNi_{0.8}Co_{0.2}O_2$ nanotubes, while Figure 7 shows that of $LiMn_2O_4$ nanotubes. All of the nanotubes are hollow with outer diameters of ~300 nm and a wall thickness of 20−30 nm. Note that the observed outside diameters of these tubes are greater than the nominal pore diameter. It has been suggested[34,35] that this occurs because the pore diameter at the surface of the membrane is less than the diameter of the pore through most of the thickness of the membrane (i.e., bottleneck pores). The nominal pore diameter is often obtained via SEM of the membrane surface, so the average pore diameter is actually larger.

HRTEM images and FFT analysis reveal the polycrystalline nature of the as-prepared nanotubes. The interlayer spacings of 0.469 nm in Figure 6c and 0.475 nm in Figure 7c are consistent with the corresponding (003) plane of $LiNi_{0.8}Co_{0.2}O_2$ and the (111) plane of $LiMn_2O_4$, respectively. It is also visible that the crystallinity of $LiNi_{0.8}Co_{0.2}O_2$ and $LiMn_2O_4$ is not as good as that of $LiCoO_2$, proving the relatively easy synthesis of $LiCoO_2$.

According to the present study, the formation of $LiCoO_2$, $LiNi_{0.8}Co_{0.2}O_2$, and $LiMn_2O_4$ nanotubes involves the steps that follow. At first, ethylene glycol reacted with inorganic salts to yield metal−organic compounds, which polymerize with each other to form a well-mixed sol at 80 °C;[36] then, the sol was introduced into template pores and the precursor gel was developed by heating. Second, the nanoparticles of intermediate phases of $Li_2CO_3$ and transition metal oxides (such as $Co_3O_4$) began to appear and form the target products along the tunnels of AAO membranes with the decomposition of the enclosed gel at a calcination temperature of about 500 °C. Finally, with the in situ reaction in progress, the nanotubes grow up to the final morphology with the combination of more and more nanoparticles.

The specific surface areas (SSA) of the as-synthesized $LiCoO_2$, $LiNi_{0.8}Co_{0.2}O_2$, and $LiMn_2O_4$ nanotubes obtained by the BET measurement were about 55, 51, and 65 $m^2/g$, respectively. These values are higher than that of the corre-

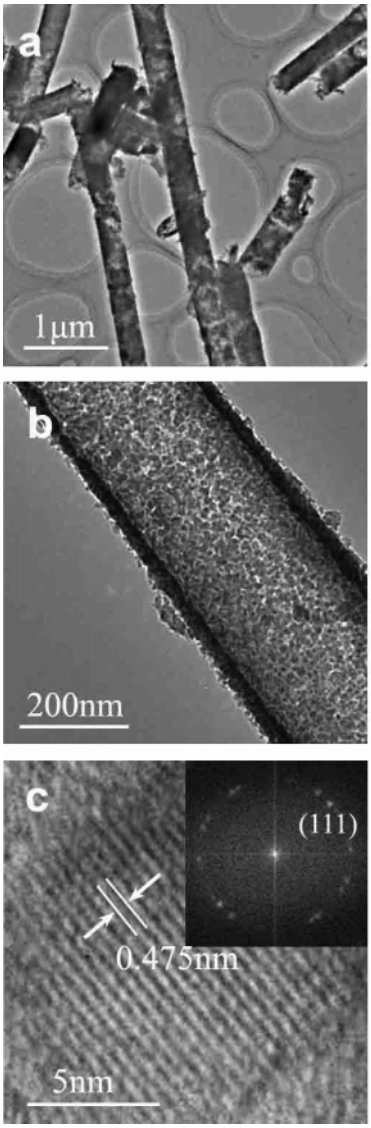


**Figure 7.** Typical TEM (a,b) and HRTEM (c) images of the as-prepared $LiMn_2O_4$ nanotube. The inset of panel c is the corresponding FFT analysis.

sponding bulk forms and nanoparticles. It has been reported that the electrode of a larger surface area can lead to a smaller effective current density during discharge than for a conventional electrode discharged at the same current density.[20,37] As a result, the as-prepared nanotubes may facilitate the electrochemical deinsertion/insertion of lithium ion and thereby improved cycling performance of the electrodes would be expected.

The charge−discharge reactions of $LiCoO_2$, $LiNi_{0.8}Co_{0.2}O_2$, and $LiMn_2O_4$ nanotube electrodes at the potential range of 3−4.3 V vs $Li/Li^+$ can be expressed by eqs 3−5, respectively.

$$LiCoO_2 \underset{\text{discharge}}{\overset{\text{charge}}{\rightleftharpoons}} xLi^+ + xe^- + Li_{(1-x)}CoO_2 \qquad (3)$$

$$LiNi_{0.8}Co_{0.2}O_2 \underset{\text{discharge}}{\overset{\text{charge}}{\rightleftharpoons}} xLi^+ + xe^- + Li_{(1-x)}Ni_{0.8}Co_{0.2}O_2 \qquad (4)$$

$$LiMn_2O_4 \underset{\text{discharge}}{\overset{\text{charge}}{\rightleftharpoons}} xLi^+ + xe^- + Li_{(1-x)}Mn_2O_4\ (0 \le x \le 1) \qquad (5)$$

CV experiments were performed to measure the reversibility of the nanostructured electrodes by first scanning from a potential of 2.5 V to an upper limit of 4.3 V and returning on the reverse scan to the original voltage. In all cases, the first to tenth voltammograms are identical to each other, and only the first scan voltammograms are present here.

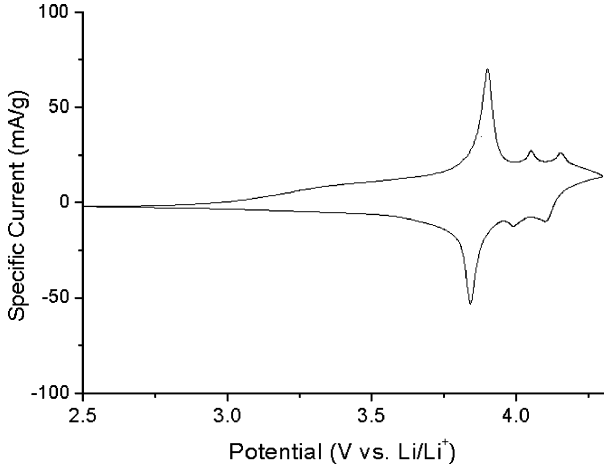


**Figure 8.** CV of $LiCoO_2$ nanotube electrode obtained at a scan rate of 1 mV/s.

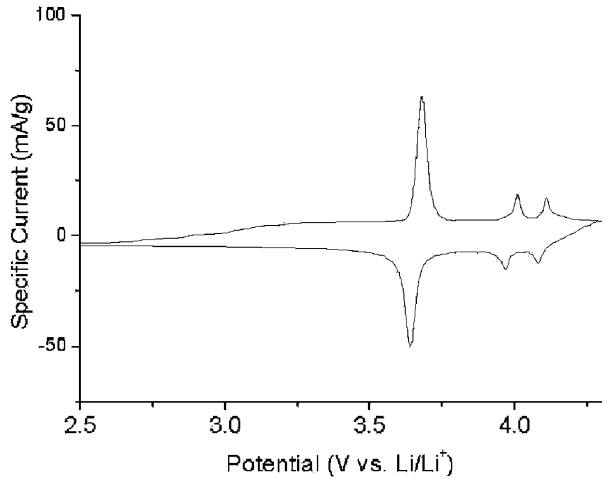


**Figure 9.** CV of $LiNi_{0.8}Co_{0.2}O_2$ nanotube electrodes; scan rate, 1 mV/s.

Figure 8 shows the CV for the $LiCoO_2$ nanotubes electrode at a scan rate of 1 mV/s. From this curve, it can be seen that three sets (cathodic, anodic) of current peaks appeared at around the potentials (V) of (3.84, 3.90), (3.99, 4.05), and (4.10, 4.15), respectively. The shape of the curve is similar to that obtained for bulk $LiCoO_2$, as reported by other researchers.[38] The first set is due to the first-order phase transition between two hexagonal phases (can also be assigned to the lithium ion deinsertion/insertion process), while the second and third sets are caused by the order−disorder phase transition.[38] The first set of peaks is much more pronounced than the following two sets and indicates that the phase transition process between ordered hexagonal phases is much more active than the order−disorder process. Moreover, the voltammetric peak separation ($\Delta E_{pk}$) value of the first set is 60 mV, equal to the ideal reversible one electron $\Delta E_{pk}$ value. Accordingly, for a $LiCoO_2$ nanotube electrode, insertion and extraction of $Li^+$, which associates with order−order phase transition, dominate the charge/discharge process and provide good redox reversibility.

The CVs of $LiNi_{0.8}Co_{0.2}O_2$ nanotube electrodes are shown in Figure 9. As typically seen over this potential window, three voltammetric waves resembling that of $LiCoO_2$ nanotubes electrodes were also observed. Differently, the relevant peaks

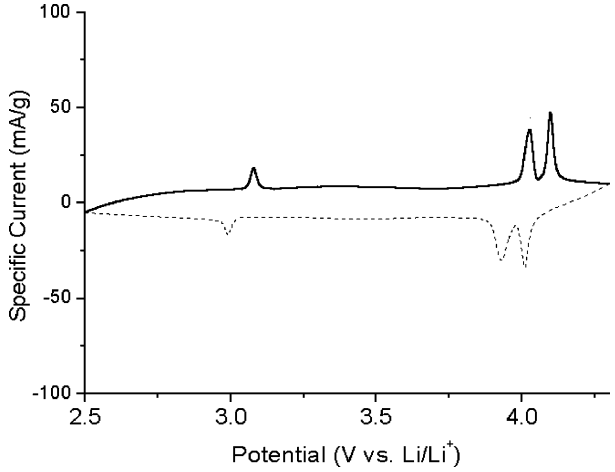


**Figure 10.** CV of $LiMn_2O_4$ nanotube electrode; scan rate, 1 mV/s.

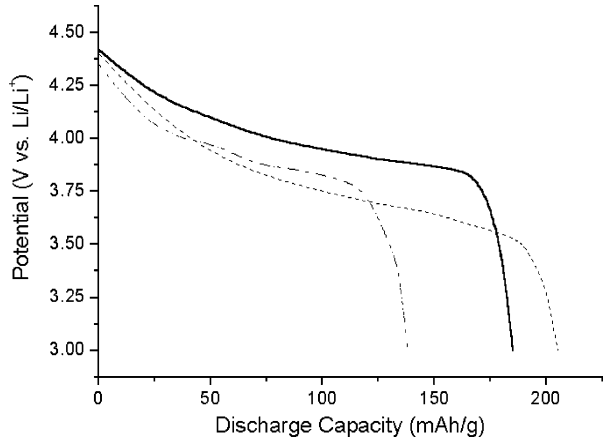


**Figure 11.** Discharge curves in the second cycle for the lithium ion cells using $LiCoO_2$ (solid), $LiNi_{0.8}Co_{0.2}O_2$ (dot), and $LiMn_2O_4$ (dash dot) nanotubes as the cathode active materials.

shifted to lower potentials. This observation indicates that the lithium ion deinsertion/insertion process occurs at more negative potentials, which makes the electrode material ($LiNi_{0.8}Co_{0.2}O_2$ nanotubes) less prone to cause corrosion and electrolyte oxidation problems.

Figure 10 is the obtained CV of the $LiMn_2O_4$ nanotube electrode. Reversible peaks were observed, but their characteristics are quite dissimilar to that of $LiCoO_2$ and $LiNi_{0.8}Co_{0.2}O_2$, which is because of the different crystal structures between them. The two sets of cathodic and anodic peaks around 4.0 and 4.1 V represent the reversible electrochemical lithium deinsertion/insertion from the tetrahedral sites of $LiMn_2O_4$, which occurs in two stages.[39] The first peak at about 4.0 V is ascribed to the removal of $Li^+$ from half of the tetrahedral sites in which Li−Li interactions exist, whereas the second peak around 4.1 V is attributed to the removal of $Li^+$ from the other tetrahedral sites where $Li^+$ do not interact. The reversible peak centered at about 3 V is due to an asymmetric lattice expansion/contraction of the $LiMn_2O_4$ electrode during the discharge/charge process. This lattice distortion is largely a result of the Jahn−Teller effect of $Mn^{3+}$ ion, which transforms the cubic crystal symmetry into tetragonal one.[8] As compared with CV data of $LiMn_2O_4$ nanoparticles and commercial $LiMn_2O_4$ powders reported by Hwang et al.,[39] the peaks of $LiMn_2O_4$ nanobubes are sharper and better-defined split, showing the higher activity of the unique tubular structure.

Figure 11 displays the discharge curves for the electrodes of $LiCoO_2$, $LiNi_{0.8}Co_{0.2}O_2$, and $LiMn_2O_4$ nanotubes recorded at the constant current density of 10 mA/g. The discharge curve of $LiCoO_2$ nanotube electrode was characterized by an initial slope at around 4.15 V and a subsequent plateau at about 3.9 V. The former is assigned to the order−disorder phase transition process, while the latter is attributed to the coexistence of two hexagonal ($\alpha$ and $\beta$) phases with slightly different lattice parameters. The $LiNi_{0.8}Co_{0.2}O_2$ nanotube electrode exhibits a similar discharge slope with relatively lower but longer plateau. The discharge curve of $LiMn_2O_4$ nanotube electrode presents two plateaus, one at 4.1 V and the other at 3.95 V. The appearance of the former plateau may be because of the coexistence of $\lambda$-$MnO_2$−$Li_{0.5}Mn_2O_4$, while the latter is due to the coexistence of two pseudophases in the form of $Li_{0.5}Mn_2O_4$−$LiMn_2O_4$. Despite the lower capacity and shorter discharge plateau, a flatter voltage response occurs in the $LiMn_2O_4$ system, which provides a very nearly constant voltage during 95% of the full discharge and hereby is ideal for the electronic memory device backup applications.

**TABLE 1: Characteristics of $LiCoO_2$, $LiNi_{0.8}Co_{0.2}O_2$, and $LiMn_2O_4$ Nanotubes as the Cathode Active Materials of Lithium Ion Batteries**

| electrode materials | molecular weight | capacity (mAh/g) theoretical | capacity (mAh/g) examined | utilization ratio[c] |
|---|---|---|---|---|
| $LiCoO_2$[a] | 97.87 | 274 | 185 | 0.67 |
| $LiCoO_2$[b] | | | 132 | 0.48 |
| $LiNi_{0.8}Co_{0.2}O_2$[a] | 97.82 | 274 | 205 | 0.75 |
| $LiNi_{0.8}Co_{0.2}O_2$[b] | | | 182 | 0.66 |
| $LiMn_2O_4$[a] | 180.8 | 148 | 138 | 0.93 |
| $LiMn_2O_4$[b] | | | 117 | 0.79 |

[a] The as-synthesized nanotubes in this work. [b] Nanoparticles reported in refs 40−44. [c] The ratio of examined capacity to theoretical capacity.

Although the charge−discharge reactions (see eq 3−5) that take place in $LiCoO_2$, $LiNi_{0.8}Co_{0.2}O_2$, and $LiMn_2O_4$ electrodes are actually complex, the capacities of these materials can be based on a reversible range of the lithium content during the charging/discharging process. For example, if $LiCoO_2$ is fully utilized with $x = 1$, its specific capacity is 274 ($26.8 \times 1000/97.87$) mAh/g. Meanwhile, the theoretical capacities of $LiNi_{0.8}Co_{0.2}O_2$ and $LiMn_2O_4$ are 274 and 148 mAh/g, respectively. By comparing the experimentally obtained capacities with the corresponding theoretical values, it can be found that utilizations of 67% for $LiCoO_2$, 75% for $LiNi_{0.8}Co_{0.2}O_2$, and 93% for $LiMn_2O_4$ were achieved. However, the values for the corresponding nanoparticles are much lower. Table 1 summarizes the contrast of capacities between the as-prepared nanotube electrodes and the nanoparticle ones. It clearly shows that the electrochemical properties of the nanotubes can provide much higher capacities than that of their corresponding nanoparticles.[40−44]

Figure 12 shows the effect of discharge current densities on the capacities of the three nanotube electrodes. The discharge capacity of each electrode decreases with increasing discharge current density. However, the decreasing rate for each electrode is different. The capacities for $LiCoO_2$, $LiNi_{0.8}Co_{0.2}O_2$, and $LiMn_2O_4$ nanotube electrodes at 10 mA/g were 185, 205, and 138 mAh/g, while at 40 mA/g, they were 163, 156, and 103 mAh/g, respectively. This means that at 40 mA/g, the capacity retentions of $LiCoO_2$, $LiNi_{0.8}Co_{0.2}O_2$, and $LiMn_2O_4$ nanotube electrodes are 88.1, 76.1, and 74.6%, respectively. Thus, the $LiCoO_2$ nanotube electrode showed a better discharge capability at higher current densities than that of $LiNi_{0.8}Co_{0.2}O_2$ and $LiMn_2O_4$, although its discharge capacity at 10 mA/g is lower than that of $LiNi_{0.8}Co_{0.2}O_2$. The capacity of $LiMn_2O_4$ nanotube electrode falls a bit more rapidly, which may be due to the

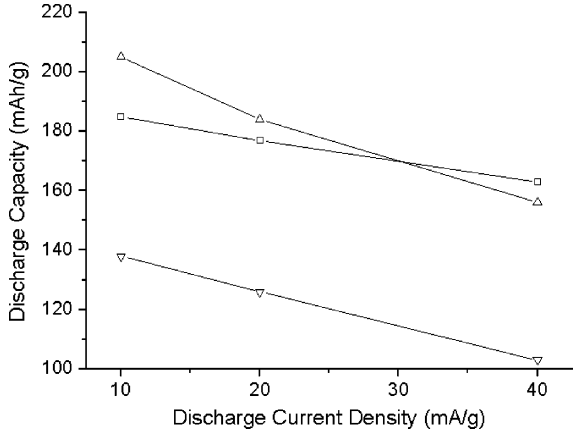


**Figure 12.** Discharge capacity vs discharge current density for $LiCoO_2$ (line with square), $LiNi_{0.8}Co_{0.2}O_2$ (line with up triangle), and $LiMn_2O_4$ (line with down triangle) nanotube electrodes.

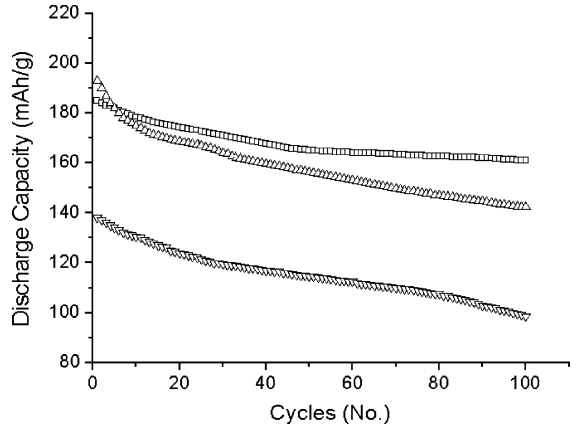


**Figure 13.** Variation of discharge capacity vs number of cycles for the lithium ion cells using $LiCoO_2$ (square), $LiNi_{0.8}Co_{0.2}O_2$ (up triangle), and $LiMn_2O_4$ (down triangle) nanotubes as the cathode electrode materials. Cycling was carried out galvanostatically at constant discharge/charge current density of 10 mA/g between 3.0 and 4.3 V.

relatively poorer crystalline of $LiMn_2O_4$ nanotubes as discussed in SEM and TEM analysis.

Figure 13 shows the cycling behaviors of the lithiated transition metal oxides nanotube electrodes. Starting from the first cycle, the discharge capacity decreased with the increase of the cycle numbers such as the case for the corresponding commercial powders and nanoparticles. It can be seen that $LiCoO_2$, $LiNi_{0.8}Co_{0.2}O_2$, and $LiMn_2O_4$ nanotubes showed an average capacity loss of 0.24, 0.49, and 0.35 mAh/g per cycle, respectively. In other words, after 100 charge−discharge cycles, the discharge capacities for the three lithiated transition metal oxide nanotubes maintain 89, 71, and 69% of their initial capacities, respectively. Hence, the electrodes made of the as-prepared nanotubes exhibit good cycling capability. In addition, an interesting and suggestive (but not conclusive) observation is that the discharge capacity of $LiCoO_2$ nanotube electrode decreased by 10% of its original value after 50 cycles, but after that, almost no further capacity was lost. The reason of such phenomena is not clear and remains to be further studied.

The above analysis presents several unique advantages to some extent for $LiCoO_2$, $LiNi_{0.8}Co_{0.2}O_2$, and $LiMn_2O_4$ nanotubes, respectively. The application of two or three kinds of these nanotubes in optimum proportions for Li ion batteries may be conducive to a combined benefit. On the other hand, the electrochemical performances of these nanotube electrodes are better than that of the nanoparticle counterparts in different

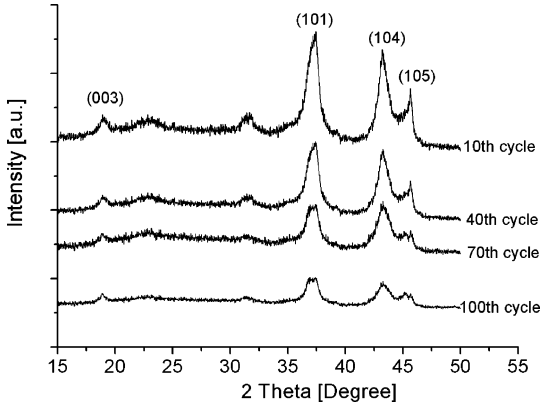


**Figure 14.** XRD patterns of the $LiNi_{0.8}Co_{0.2}O_2$ samples taken from the cathode mix of tested cell after different discharge/charge cycles. The samples were calcined at 400 °C in air to dispose of the carbon in cathode mix. The XRD patterns at various cycles exhibit similar diffraction lines to the initial XRD spectra of the sample before electrochemical measurement, indicating that the main crystal structure is preserved during electrochemical cycling.

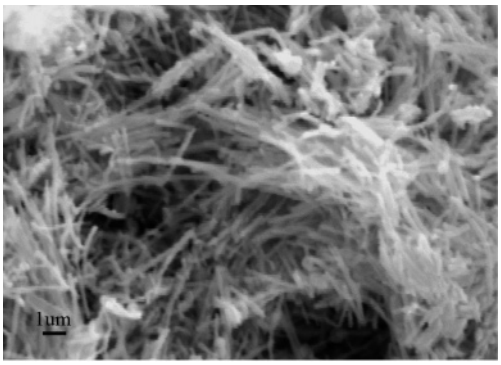


**Figure 15.** SEM image of the cathod mix removed from the $LiNi_{0.8}Co_{0.2}O_2$ nanotube electrode after 100 charge/discharge cycles. Because of the presence of carbon and binding agent in the cathode mix, the SEM image is not clear enough to identify the specific nanotube structrue. However, this image can show that the 1D nanosize morphology of the lithium transition metal oxide was preserved during the lithium insertion/deinsertion process.

degrees. To further understand the characteristics of the nanotubes electrodes, XRD spectra and SEM images were taken for the $LiNi_{0.8}Co_{0.2}O_2$ electrode during various stages of the discharge/charge process. All XRD patterns of the $LiNi_{0.8}Co0.2O_2$ samples removed from the tested cell after different lithium insertion/deinsertion cycles (Figure 14) exhibit similar diffraction lines, showing that the main crystal structure is preserved during electrochemical cycling. At the same time, the main diffraction peaks of the samples show slight variations in width, which is attributed to the cell parameters change of the $LiNi_{0.8}Co_{0.2}O_2$ phases. However, this change is very small, so the loss of the cell capacity can be limited to a narrow range.

Meanwhile, the SEM image of the cathode mixture (Figure 15) shows that, after 100 discharge/charge cycles, $LiNi_{0.8}Co_{0.2}O_2$ still preserves the one-dimensional (1D) nanostructure. It was reported that no obvious crystal structure change was observed during various lithium intercalation stages in a charge−discharge cycle.[45] Thus, the primary crystal structure and 1D nanosize morphology of $LiNi_{0.8}Co_{0.2}O_2$ are retained during cycling process, which is important for holding the capacity of the batteries.

We believe the significantly improved electrochemical properties of the nanotubes electrode may result from the following two effects. One is the relatively high specific surface areas of

hollow tubular structures, which offer more active positions for lithium ion intercalating/deintercalating and lower the real current density.[20] Another factor concerns faster kinetics related to nanotubular structure of electrode. The thickness of the tubes (20−30 nm) is much less than the radii of the corresponding commercial spheres or nanocrytallines, resulting in a higher diffusion rate and significantly faster electronic kinetics.[17] Furthermore, the tubular structure is relatively flexible during discharge/charge cycles. In a word, the hollow structure of the nanotube, which allows the solid state diffusion and intercalation/deintercalation to occur easily, contributes to higher capacities and better reversibility. Thus, lithiated transition metal oxides with 1D nanostructures are promising positive materials in lithium ion batteries as described above. However, it is impracticable to mass produce them with AAO membranes in commercial use. The main purpose of employing the AAO membrane to synthesize nanotubes in this paper is, from a point view of fundamental studies and a concern for the emerging field of microbatteries, to estimate the unique electrochemical performance of lithiated transition metal oxides with nanotube structures. To take advantage of nanotube electrodes in future applications, a method of nanotube mass production is needed, which is of great scientific and applied importance. A close approach could be the surfactant-directed hydrothermal growth or templateless assembly in soft solution process. Recently, some progress has been made in synthesizing nanobelts of $LiMn_2O_4$[46] and nanotubes of $VO_x$[47,48] with a low temperature hydrothermal method. Further work including the preparation and electrochemical analysis is full of challenges and has a chance to be investigated in the future.

## Conclusions

We have demonstrated that open-ended nanotubes of layered $LiCoO_2$, doped $LiNi_{0.8}Co_{0.2}O_2$, and spinel $LiMn_2O_4$ were prepared on the basis of the obtained bulk by combined template synthesis and thermal decomposition. The template-assisted growth process yielded large scale nanotubes with uniform sizes and shapes. An "in situ reacted nanoparticle nanotube" formation mechanism was presented. Electrochemical measurement showed that the as-synthesized nanotube electrodes could be charged and discharged reversibly with high capacities and good rate capabilities. In view of this special structural arrangement, it is confirmed that intercalation−deintercalation cycles could be more efficiently conducted with the tubular organized lithiated transition metal oxides than that of the nanocrystalline counterparts to different extents. The enhanced electrochemical character of nanotube electrodes arises from their relatively high specific surface areas and short $Li^+$ solid state diffusion lengths. Therefore, nanotubes of those lithiated transition metal oxides are promising positive electrode materials in lithium ion batteries.

**Acknowledgment.** This work was supported by the National NSFC (20325102 and 90406001) and MOE-Key Project (104055).

## References and Notes

(1) Linden, D.; Reddy, T. B. *Handbook of Batteries*, 3rd ed.; McGraw-Hill Inc.: New York, 2002.
(2) Tarascon, J. M.; Armand, M. *Nature* **2001**, *414*, 359.
(3) Whittingham, M. S. *Chem. Rev.* **2004**, *104*, 4271.
(4) Ronci, F.; Scrosati, B.; Rossi, A. V.; Perfetti, P. *J. Phys. Chem. B* **2001**, *105*, 754.
(5) Besenhard, J. O. *Handbook of Battery Materials*; Wiley-VCH: New York, 1999.
(6) Murphy, D. W.; DiSalvo, F. J.; Carides, J. N.; Waszczak, J. V. *Mater. Res. Bull.* **1978**, *13*, 1395.
(7) Lazzari, M.; Scrosati, B. *J. Electrochem. Soc.* **1980**, *127*, 773.
(8) Winter, M.; Besenhard, J. O.; Spahr, M. E.; Novak, P. *Adv. Mater.* **1998**, *10*, 725.
(9) Thomas, M. G. S. R.; Bruce, P. G.; Goodenough, J. B. *Solid State Ionics* **1986**, *18−19*, 749.
(10) Campbell, S. A.; Bows, C.; McMillan, R. S. *J. Electroanal. Chem.* **1990**, *284*, 195.
(11) Dahn, J. R.; Von Sacken, U.; Juzkow, M. W.; Al-Janaby, H. *J. Electrochem. Soc.* **1991**, *138*, 2207.
(12) Ohzuku, T.; Ueda, A.; Nagayama, M.; Iwakoshi, Y.; Komori, H. *Electrochim. Acta* **1993**, *38*, 1159.
(13) Jing, L. L.; Frank, M.; Robert, K. *J. Phys. Chem. B* **2005**, *109*, 952.
(14) Park, H.-S.; Hwang, S.-J.; Choy, J.-H. *J. Phys. Chem. B* **2001**, *105*, 4860.
(15) Kovacheva, D.; Gadjov, H.; Petrov, K.; Mandal, S.; Lazarraga, M. G.; Pascual, L.; Amarilla, J. M.; Rojas, R. M.; Herrero, P.; Rojo, J. M. *J. Mater. Chem.* **2002**, *12*, 1184.
(16) Pistoia. *Lithium Batteries: New Materials, Development and Perspectives*; Elsevier: Amsterdam, 1994.
(17) Yu, L. H.; Yang, H. X.; Ai, X. P.; Cao, Y. L. *J. Phys. Chem. B* **2005**, *109*, 1148.
(18) Tarascon, J. M.; Wang, E.; Shokoohi, F. K.; McKinnon, W. R.; Colson, S. *J. Electrochem. Soc.* **1991**, *138*, 2859.
(19) Kumar, V. G.; Gnanaraj, J. S.; Ben-David, S.; Pickup, D. M.; van-Eck, E. R. H.; Gedanken, A.; Aurbach, D. *Chem. Mater.* **2003**, *15*, 4211.
(20) Nishizawa, M.; Mukai, K.; Kuwabata, S.; Martin, C. R.; Yoneyama, H. *J. Electrochem. Soc.* **1997**, *144*, 1923.
(21) Wang, Y.; Takahashi, K.; Shang, H. M.; Cao, G. Z. *J. Phys. Chem. B* **2005**, *109*, 3085.
(22) Zhou, Y. K.; Huang, J.; Shen, C. M.; Li, H. L. *Mater. Sci. Eng., A* **2002**, *335*, 260.
(23) Zhou, Y. K.; Shen, C. M.; Li, H. L. *Solid State Ionics* **2002**, *146*, 81.
(24) Zhou, Y. K.; Shen, C. M.; Huang, J.; Li, H. L. *Mater. Sci. Eng., B* **2002**, *95*, 77.
(25) Sui, Y. C.; Acosta, D. R.; González-León, J. A.; Bermúdez, A.; Feuchtwanger, J.; Cui, B. Z.; Flores, J. O.; Saniger, J. M. *J. Phys. Chem. B* **2001**, *105*, 1523.
(26) Wirtz, M.; Parker, M.; Kobayashi, Y.; Martin, C. R. *Chem. Eur. J.* **2002**, *8*, 3572.
(27) Chen, J.; Tao, Z. L.; Li, S. L. *J. Am. Chem. Soc.* **2004**, *126*, 3060.
(28) Adhikary, K.; Takahashi, M.; Kikkawa, S. *Mater. Res. Bull.* **1998**, *33*, 1845.
(29) Nakamura, T.; Kajiyama, A. *Solid State Ionics* **1999**, *123*, 95.
(30) Lee, Y.-S.; Sun, Y.-K.; Nahm, K.-S. *Solid State Ionics* **1998**, *109*, 285.
(31) Liu, Z. Q.; Wang, W. L.; Liu, X. M.; Wu, M. C.; Li, D.; Zeng, Z. *J. Solid State Chem.* **2004**, *177*, 1585.
(32) Liu, H. S.; Zhang, Z. R.; Gong, Z. L.; Yang, Y. *Solid State Ionics* **2004**, *166*, 317.
(33) Tao, S. W.; Wu, Q. Y.; Zhan, Z. L.; Meng, G. Y. *Solid State Ionics* **1999**, *124*, 53.
(34) Schonenberger, C.; Zane, B. M. I.; Fokkink, L. G. J.; Henny, M.; Schmid, C.; Kruger, M.; Bachtold, A.; Huber, R.; Birk, H.; Staufer, U. *J. Electrochem. Soc.* **1997**, *101*, 5497.
(35) Jirage, K. B.; Hulteen, J. C.; Martin, C. R. *Science* **1997**, *278*, 655.
(36) Han, Y. S.; Kim, H. G. *J. Power Sources* **2000**, *88*, 161.
(37) Che, G. L.; Jirage, K. B.; Fisher, E. R.; Martin, C. R. *J. Electrochem. Soc.* **1997**, *144*, 4296.
(38) Shin, H.-C.; Pyun, S. I. *Electrochim. Acta* **2001**, *46*, 2477.
(39) Huang, B. J.; Santhanam, R.; Liu, D. G. *J. Power Sources* **2001**, *97−98*, 443.
(40) Hon, Y. M.; Fung, K. Z.; Lin, S. P.; Hon, M. H. *J. Solid State Chem.* **2002**, *163*, 231.
(41) Liang, H. Y.; Qiu, X. P.; Chen, H. L.; He, Z. Q.; Zhu, W. T.; Chen, L. Q. *Electrochem. Commun.* **2004**, *6*, 789.
(42) Chen, H. L.; Qiu, X. P.; Zhu, W. T.; Hagenmuller, P. *Electrochem. Commun.* **2002**, *4*, 488.
(43) Liang, H. Y.; Qiu, X. P.; Zhang, S. C.; He, Z. Q.; Zhu, W. T.; Chen, L. Q. *Electrochem. Commun.* **2004**, *6*, 505.
(44) Richard, K. B.; Gover, R. K.; Brian, J. M.; Hirano, A.; Kawamoto, Y. *J. Power Sources* **2001**, *97−98*, 316.
(45) Saadoune, I.; Delmas, C. *J. Solid State Chem.* **1998**, *136*, 8.
(46) Zhang, L. Z.; Yu, J. C.; Xu, A. W.; Li, Q.; Kwong, K. W.; Wu, L. *Chem. Commun.* **2003**, *23*, 2910.
(47) Chandrappa, G. T.; Steunou, N.; Cassaignon, S.; Bauvais, C.; Livage, J. *Catal. Today* **2003**, *78*, 85.
(48) Chen, W.; Peng, J. F.; Mai, L. Q.; Zhu, Q. Y.; Xu, Q. *Mater. Lett.* **2004**, *58*, 2275.